ACS NANO

www.acsnano.org

ARTICLE

# Ultrasensitive Electrochemical Detection of Mutated Viral RNAs with Single-Nucleotide Resolution Using a Nanoporous Electrode Array (NPEA)

Jinho Yoon, Brian M. Conley, Minkyu Shin, Jin-Ha Choi, Cemile Kilic Bektas, Jeong-Woo Choi,* and Ki-Bum Lee*

Cite This: https://doi.org/10.1021/acsnano.1c10824

Read Online

ACCESS | Metrics & More | Article Recommendations | Supporting Information

**ABSTRACT:** The detection of nucleic acids and their mutation derivatives is vital for biomedical science and applications. Although many nucleic acid biosensors have been developed, they often require pretreatment processes, such as target amplification and tagging probes to nucleic acids. Moreover, current biosensors typically cannot detect sequence-specific mutations in the targeted nucleic acids. To address the above problems, herein, we developed an electrochemical nanobiosensing system using a phenomenon comprising metal ion intercalation into the targeted mismatched double-stranded nucleic acids and a homogeneous Au nanoporous electrode array (Au NPEA) to obtain (i) sensitive detection of viral RNA without conventional tagging and amplifying processes, (ii) determination of viral mutation occurrence in a simple detection manner, and (iii) multiplexed detection of several RNA targets simultaneously. As a proof-of-concept demonstration, a SARS-CoV-2 viral RNA and its mutation derivative were used in this study. Our developed nanobiosensor exhibited highly sensitive detection of SARS-CoV-2 RNA (~1 fM detection limit) without tagging and amplifying steps. In addition, a single point mutation of SARS-CoV-2 RNA was detected in a one-step analysis. Furthermore, multiplexed detection of several SARS-CoV-2 RNAs was successfully demonstrated using a single chip with four combinatorial NPEAs generated by a 3D printing technique. Collectively, our developed nanobiosensor provides a promising platform technology capable of detecting various nucleic acids and their mutation derivatives in highly sensitive, simple, and time-effective manners for point-of-care biosensing.

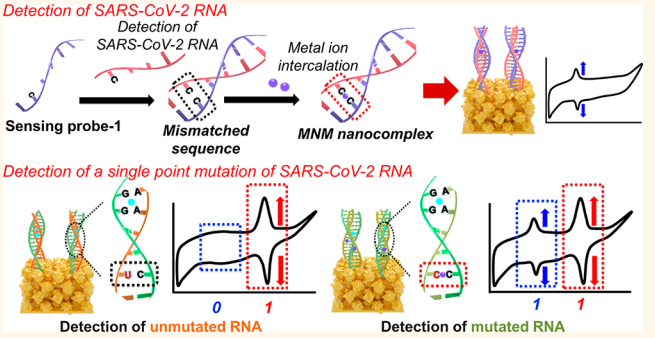


**KEYWORDS:** *electrochemical nanobiosensors, detection of nucleic acids, detection of single point mutation, mismatched nucleic acid−metal ion (MNM) nanocomplex, nanoporous electrode array (NPEA), multiplexed detection, SARS-CoV-2*

Nucleic acids, such as mRNA, microRNA, small interfering RNA (siRNA), and DNA, are essential biomolecules to all life forms, and various types of nucleic acids play essential roles in the maintenance of living organisms.[1,2] Thereby, detecting the expression level of target nucleic acids is critical for many biomedical applications and essential for health surveillance to diagnose diseases such as cancers.[3−6] In addition, rapid and accurate detection of infectious viral DNAs and RNAs, which have recently received attention because of coronavirus disease 2019 (COVID-19), enables us to prevent widespread infections promptly.[7,8] Detecting targeted viral nucleic acids has advantages over detecting other viral biomarkers, such as membrane proteins, spike glycoproteins, and nucleocapsid proteins, as nucleic acids can be used to more easily determine mutations, a challenge for other biomarkers.[9,10]

To this end, various biosensing techniques have been established to detect nucleic acids, such as viral RNAs and DNAs, including fluorescence-based techniques and surface-enhanced Raman spectroscopy (SERS)-based techniques.[11−14] Although each technique has advantages for detecting nucleic

Received: December 6, 2021
Accepted: March 29, 2022

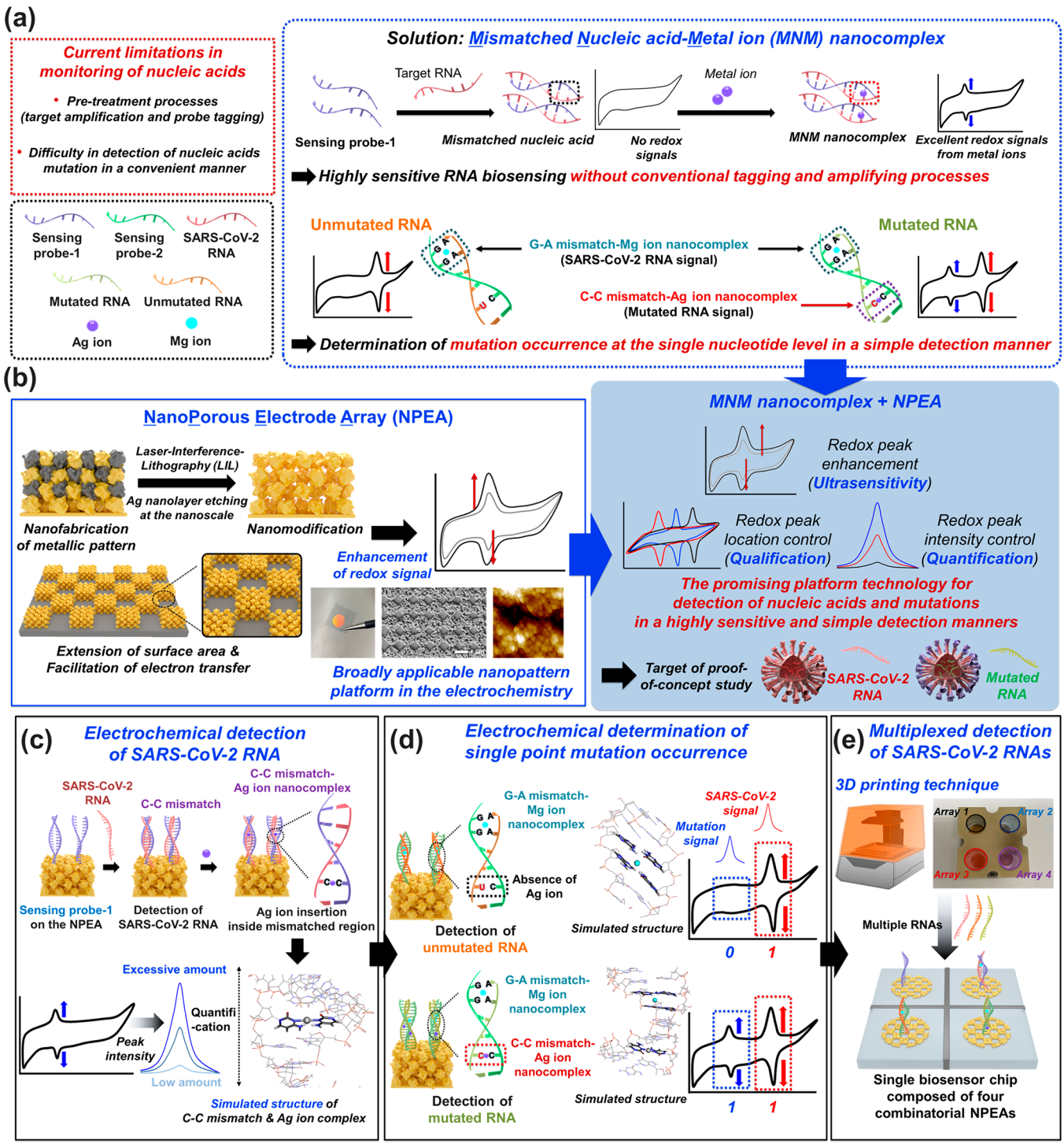


**Figure 1. Electrochemical SARS-CoV-2 nanobiosensor using mismatched nucleic acid−metal ion nanocomplex on a Au NPEA. (a) Schematic diagram of nucleic acid biosensing mechanism using mismatched nucleic acids−metal ion (MNM) nanocomplex formation for highly sensitive SARS-CoV-2 RNA detection and electrochemical determination of single point mutation occurrence and its broad applicability in multiplexed detection of various nucleic acids. (b) Scheme and optical image of the Au NPEA. (c) Electrochemical detection of target single SARS-CoV-2 RNA. (d) Electrochemical determination of single point mutation occurrence in SARS-CoV-2 RNA using two different types of mismatched nucleic acids and metal ions. (e) Schematic diagram of multiplexed detection of several SARS-CoV-2 RNAs on a single biosensor chip composed of combinatorial Au NPEAs fabricated by a 3D printing technique.**

acids, they require several additional pretreatments (*e.g.*, nucleic acid amplification) on the biological samples before their detection steps. For instance, target DNA amplification is typically used to achieve high sensitivity, and several techniques require expensive equipment and expert technicians for operation.[15,16] Besides, since nucleic acids have no inherent characteristics for demonstration of each biosensing technique, additional tagging processes of probe molecules should be required by introducing redox molecules, fluorescence dyes, or Raman-active molecules on nucleic acids that inevitably require


https://doi.org/10.1021/acsnano.1c10824
ACS Nano XXXX, XXX, XXX−XXX

time and extra costs.[17−19] Thus, these pretreatments have hindered their application to point-of-care (POC) biosensing, which is recognized as a standard for next-generation biosensors.[20,21] POC biosensing is drawing increasing attention, as it provides rapid, convenient, and simple detection for measuring infectious diseases' nucleic acids. Likewise, as observed with the recent issues of severe acute respiratory syndrome coronavirus 2 (SARS-CoV-2) mutations, it is crucial to determine the occurrence of mutations in nucleic acids, particularly single point mutation, which has been limited using current biosensors reported so far.[22,23] Therefore, there is an urgent need to develop a method to detect nucleic acids without conventional target amplification and tagging processes, all of which can enable us to detect the occurrence of mutations rapidly and straightforwardly.

Addressing the challenges above, we developed an electrochemical nucleic acid nanobiosensor to achieve (i) highly sensitive detection of nucleic acids without conventional tagging, and target amplification, (ii) accurate determination of viral single point mutation occurrence, and (iii) multiplexed detection of several target nucleic acids on the combinatorial nanopatterns. As a proof-of-concept, SARS-CoV-2 viral RNA and its mutation derivative were selected for this study. Electrochemical biosensors have been widely recognized for their potential in POC sensing applications.[24,25] However, the low electrochemical sensitivity of conventional electrodes has limited electrochemical biosensor-based early detection of viral diseases. To address this issue, we introduced a homogeneous Au nanoporous electrode array (NPEA) as an electrode with a high surface-area-to-volume ratio that can provide faster electron transfer and can improve efficient mass transfer compared to conventional electrodes, in that way significantly enhancing electrochemical output.[26,27] Additionally, our nanoarray is fabricated by a high-throughput laser interference lithography (LIL) approach, which improves the uniformity and reproducibility of our electrochemical biosensors.[28,29]

Besides, to solve the drawback of conventional tagging and target amplification for nucleic acid biosensing, we employed a phenomenon that converts genetic information (*e.g.*, RNA sequences) into electrochemical signals using metal ion intercalation into mismatched double-stranded nucleic acids.[30,31] It has been known that specific redox metal ions can selectively and effectively intercalate into mismatched sequences in double-stranded nucleic acids under physiologically relevant conditions to stabilize the mismatched sequences by the formation of a mismatched nucleic acid−metal ion (MNM) nanocomplex.[32,33] Using this phenomenon, we designed the sensing probe to form the intended types and numbers of mismatched sequences by hybridizing with target RNA. After detecting the target sequence, intercalated redox metal ions in the mismatched sequences are used as the redox probe directly to remove the conventional probe tagging. The high sensitivity could be achieved without target amplification due to intercalated metal ions' outstanding redox property (Figure 1a). Besides, by combining with NPEA, the redox signals from intercalated metal ions are enhanced more (Figure 1b). As different metal ions with intrinsic oxidation peaks can specifically bind to other mismatches, we further realized the determination of the single point mutation of RNA by simply combining two types of mismatched sequences and metal ions. Using this biosensing process, SARS-CoV-2 RNA can be detected electrochemically on the sensing probe-immobilized NPEA in a highly sensitive and quantitative manner (Figure 1c). The determination of the mutation of SARS-CoV-2 RNA can be achieved at the single-nucleotide level by combining two types of mismatched sequences and different metal ions (Figure 1d). In addition to electrochemical verification and theoretical support, we also conducted the structural simulation of MNM nanocomplex formation to support our hypothesis.[34,35] Finally, using a single biosensor chip composed of four combinatorial NPEAs, multiplexed detection of several SARS-CoV-2 RNAs was successfully conducted by introducing a 3D-printed chamber and modifying sensing probes on each NPEA (Figure 1e).

Taken together, the highly sensitive detection of target RNA and accurate determination of whether a mutation at the single-nucleotide level with no tagging and amplifying processes could be achieved by the synergistic effects of the MNM nanocomplex and our developed NPEA-based biosensor. Furthermore, since metal ions have their own intrinsic redox peak locations and numbers of metal ions determine a peak intensity, our nanobiosensor provides a platform technology that can be broadly applicable to determine and distinguish the various viral RNAs and their mutation derivatives simultaneously by designing a sensing probe capable of forming predetermined mismatched sequences and introduction of several other metal ions.[31,34,36]

## RESULTS AND DISCUSSION

**Mismatched Nucleic Acid−Metal Ion Nanocomplex for Label and Amplification-Free RNA Biosensing and Determination of Single Point Mutation Occurrence.** To detect nucleic acids without conventional probe tagging and target amplification, we took advantage of a natural phenomenon in which specific redox-active metal ions can intercalate in mismatched sequences in double-stranded nucleic acids to stabilize the mismatched sequences by the formation of an MNM nanocomplex through covalent bonding.[32,33] For example, when a cytosine−cytosine (C−C) mismatched sequence exists in the double-stranded nucleic acids, a Ag ion can intercalate in the C−C mismatched site through covalent bonding to stabilize the mismatched sequence. In addition, intercalated Ag ions exhibit excellent redox characteristics, which can be used as a redox probe. Similarly, Mg and Hg ions can intercalate inside other mismatches, such as guanine−adenine (G−A) and thymine−thymine (T−T), respectively, to form other types of MNM nanocomplexes through covalent bonding.[31,34,36] A prerequisite for this biosensor is that we need to know the target sequence. On the basis of the target sequence, we can design the sensing probe that can hybridize with the target sequence and form an intended mismatched sequence for metal ion intercalation. The confirmation of the target detection can be decided depending on the presence or absence of the redox signals of the intercalated metal ion. Herein, a sensing probe was designed to further utilize this phenomenon for SARS-CoV-2 RNA biosensing to form one C−C mismatched sequence in double-stranded nucleic acids composed of a sensing probe and SARS-CoV-2 RNA after detection of SARS-CoV-2 RNA. After Ag ion intercalation inside the C−C mismatched sequence, an intercalated Ag ion was used as an excellent redox probe directly to evaluate SARS-CoV-2 RNA detection electrochemically. Because of the exceptional redox property of intercalated Ag ions and their rapid intercalation within 1 h under ambient conditions, highly sensitive electrochemical RNA detection can be achieved without


https://doi.org/10.1021/acsnano.1c10824
ACS Nano XXXX, XXX, XXX−XXX

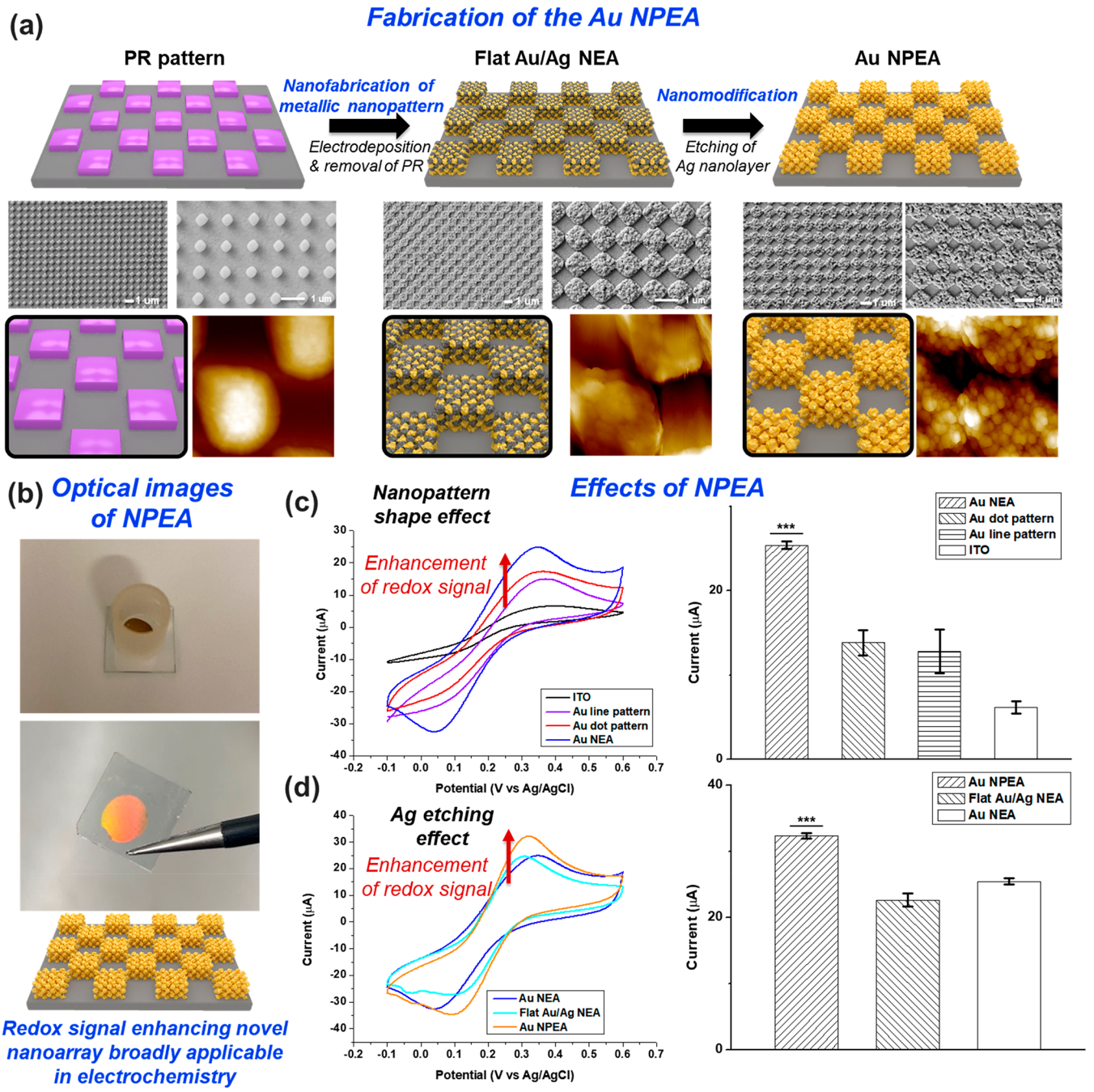


**Figure 2. Surface morphology of the Au NPEA and its characteristics. (a) Comparison of surface morphologies of the PR pattern, flat Au/Ag NEA, and Au NPEA. (b) Optical image of the prepared Au NPEA on the ITO and 3D-printed chamber-attached Au NPEA. (c) Cyclic voltammograms and oxidation current peak intensities of the Au NEA, Au line pattern, Au dot pattern, and bare ITO to confirm the redox signal enhancing effect of the chess-table-like nanostructure. Error bars show the standard error of the mean of six measurements. ***$p$ < 0.001, Student's unpaired $t$ test. (d) Cyclic voltammograms and oxidation current peak intensities of the Au NPEA, flat Au/Ag NEA, and Au NEA to confirm the Ag etching effect for redox signal enhancement. Error bars show the standard error of the mean of six measurements. ***$p$ < 0.001, Student's unpaired $t$ test.**

probe tagging and target amplification.[37] On the other hand, in the absence of SARS-CoV-2 RNA or in the presence of nontarget RNA, there is no formation of mismatched double-stranded nucleic acids; thus, no metal ions can be intercalated, and no redox signals are measured. Using this MNM nanocomplex-assisted biosensing mechanism, we designed and functionalized Au NPEA with a DNA-sensing probe (sensing probe-1), and, in the presence of SARS-CoV-2 RNA, it formed the C−C mismatched sequence and formed the C−C mismatch−Ag ion nanocomplex after Ag ion intercalation. The redox signals from the C−C mismatch−Ag ion nanocomplex were ultrasensitively measured to quantify and qualify the SARS-CoV-2 RNA electrochemically owing to the excellent redox property of Ag ions and redox signal enhancing effect of the Au NPEA (Figure 1c).

Moreover, as several metal ions can specifically intercalate into different mismatches, the sequence information on different nucleic acids can be distinguished electrochemically


https://doi.org/10.1021/acsnano.1c10824
ACS Nano XXXX, XXX, XXX−XXX

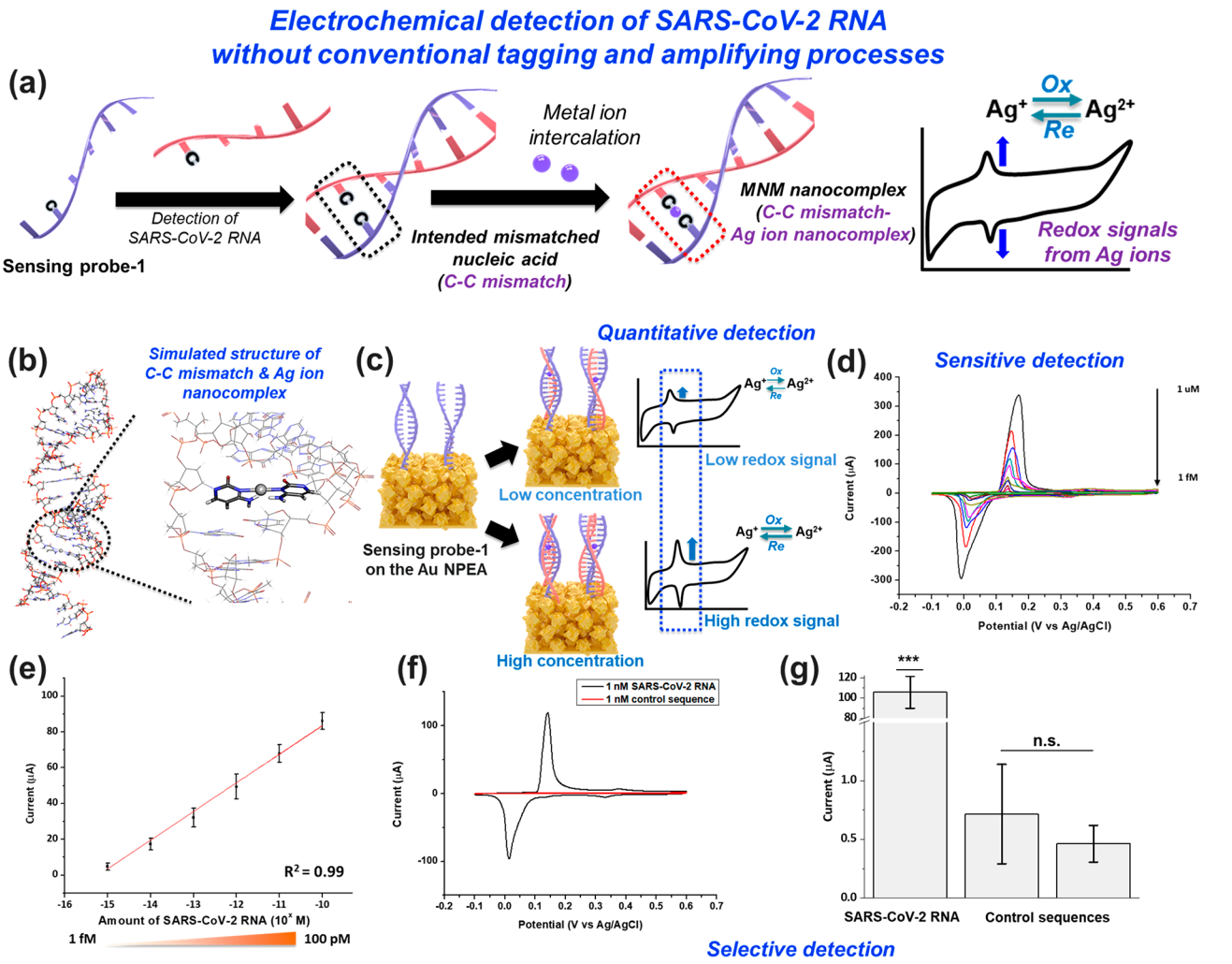


**Figure 3. Electrochemical detection of target single SARS-CoV-2 RNA. (a) Scheme of electrochemical RNA sensing using the MNM nanocomplex. (b) Simulated structure and zoomed-in structure of the MNM nanocomplex composed of SARS-CoV-2 RNA, sensing probe-1, and Ag ions. (c) Scheme for electrochemical quantification of target single SARS-CoV-2 RNA using redox signal intensities from intercalated Ag ions. (d) Cyclic voltammograms upon addition of target single SARS-CoV-2 RNA from 1 $\mu$M to 1 fM to sensing probe-1-modified Au NPEA. (e) Linear response graph of the nanobiosensor upon addition of target single SARS-CoV-2 RNA from 100 pM to 1 fM. Error bars show the standard error of the mean of three measurements. (f) Cyclic voltammograms of the nanobiosensor in the presence of target single SARS-CoV-2 RNA and control sequence. (g) Oxidation current peak intensities of the nanobiosensor in the presence of target single SARS-CoV-2 RNA and control sequences calculated from cyclic voltammograms. Error bars show the standard error of the mean of three measurements. ***$p$ < 0.001, n.s.: not significant, Student's unpaired $t$ test.**

at a single-nucleotide level by using the sensing probe capable of forming different mismatched sequences depending on the target sequences. To realize this concept for the determination of the single point mutation of the SARS-CoV-2 RNA, we introduced two types of mismatched sequences (C−C and G−A) and metal ions (Ag and Mg ions) in MNM nanocomplex-assisted biosensing.[34,36] Those mismatched sequences and metal ions were selected because they satisfied the prerequisites that they could form mismatched sequences between DNA (sensing probe) and RNA (target), and redox peak location of metal ions should be separated sufficiently from each other for accurate electrochemical measurement.[34,35,38] As a proof-of-concept study, the D614G mutation inducible SARS-CoV-2 RNA (mutated RNA) was selected because it has been the dominant variant of SARS-CoV-2 in the early stage of the pandemic, and alpha or delta mutations, which have mainly occurred recently, also possess the D614G spike mutations.[39] This mutation was generated when the 24301st sequence in the entire viral SARS-CoV-2 RNA was transformed from uracil (U) to C.

To determine the occurrence of this mutation, another sensing probe (sensing probe-2) was designed, which can be hybridized with both unmutated RNA and single point mutated RNA, but forming different mismatched sequences. Thus, as shown in Figure 1a, sensing probe-2 formed one G−A mismatched sequence with both RNAs for Mg ion intercalation, and the redox signal from intercalated Mg ion informed the existence of SARS-CoV-2 RNA with the appearance of a Mg peak defined as the "1" state (On state). However, in the presence of mutated RNA, an additional C−C mismatched sequence was formed between sensing probe-2 and single point mutated RNA for Ag ion intercalation, and redox signal from the intercalated Ag ion informed the mutation occurrence in SARS-CoV-2 RNA from U to C with the appearance of a Ag peak ("1" state). In contrast, in the presence of unmutated RNA, the Ag peak did not appear and


https://doi.org/10.1021/acsnano.1c10824
ACS Nano XXXX, XXX, XXX−XXX

was therefore considered as the "0" state (Off state). Besides, since metal ions have intrinsic redox peak locations, redox peaks from Ag and Mg ions can be easily distinguished even when they are closely located in the MNM nanocomplex. Taking advantage of this biosensing method, electrochemical determination of single point mutation occurrence was achieved by selective detection of single point mutated RNA and unmutated RNA in a simple detection event (Figure 1d).[40,41] Notably, besides the simple verification of a single point mutation occurrence, our developed biosensing strategy can provide a way to reveal the specified oligonucleotide information on a single point mutated nucleotide. Information of all nucleic acid sequences and the structures of the mismatched double-stranded nucleic acids used in the study are provided in the Materials and Methods and Table S1.

**Development of the Au NPEA to Enhance Redox Signals of the MNM Nanocomplex for Achieving Ultrasensitivity.** To enhance electrochemical detection sensitivity and biosensing reliability, highly conductive and uniform electrodes with a high surface-area-to-volume ratio are required to efficiently immobilize sensing probes and facilitate electron transfer of redox molecules. To this end, homogeneous Au NPEA was designed and developed by tuning nanostructures through several delicate approaches to significantly increase the surface-area-to-volume ratio and enhance the redox signals of the MNM nanocomplex (Figure 2a). First, a photoresist (PR) was patterned on the ITO by Lloyd's mirror interferometer (nanopattern size and the interval between adjacent nanopatterns: 800 nm, respectively) to form the periodic PR pattern used as the template for making conductive nanopatterns. In the same area, the chess-table-like nanopattern provides a larger surface-to-volume ratio than the other nanostructures such as line, dot, and grid shape; thus, the PR pattern was prepared with a dot pattern to make the conductive chess-table-like nanopatterns in further steps. The conditions for the PR pattern were optimized by controlling the developing time, and the optimized condition (23 s) showed the uniformly periodic PR pattern on the ITO with reliable structures and fully exposed ITO surface used for conductive nanopattern formation (Figures 2a, S1, and S2).

Next, using the 3D-printed hole chamber attached to the PR pattern, electrochemical deposition of Au and Au/Ag was conducted to fabricate the metallic bottom region and chess-table-like flat Au/Ag nanoelectrode array (NEA) (Figure S3). After removal of the PR, the flat Au/Ag NEA was formed reproducibly on the indium tin oxide (ITO). It showed the chess table nanostructures with a flat surface composed of connected Au/Ag nanopatterns with 200 nm height and 800 nm size by atomic force microscopy (AFM) and energy-dispersive X-ray spectroscopy (EDS) analysis (Figures S6 and S7). Finally, after removing the Ag nanolayer on the flat Au/Ag NEA by a Ag etching solution, the Au NPEA was successfully fabricated on the ITO (Figures 2a and S5). The Au NPEA showed the rough nanoclusters on the chess-table-like nanopatterns with hugely increased surface roughness and the removal of Ag nanolayers, which was further verified by EDS. The prepared Au NPEA displayed the uniform homogeneous nanocluster patterns on a large area. In addition, the electrochemically deposited area retained its region well even after strong acidic solution treatment for Ag etching (Figure 2b). The ratio of Au and Ag in the mixture was optimized as 6:1 to make the Au NPEA because a too high or low ratio of Ag affected the overall nanostructures because of the total area of the deposited Ag nanolayer, which was determined based on the electrochemical deposition velocity of Au and Ag (Figure S4).

Next, the redox signal enhancing property of Au NPEA was confirmed by cyclic voltammetry (CV) using the electrolyte prepared with redox molecules. As shown in Figure 2c, the Au NEA prepared with only Au deposition showed the increased redox peaks (oxidation peak current: 25.4 $\mu$A) compared to the other nanostructured Au patterns (14.5, 12.8, and 6.2 $\mu$A for Au grid, Au line, and bare ITO, respectively), which proved that the chess-table-like nanostructure provided an extended surface area of nanopatterns. Moreover, after Ag layer removal, the Au NPEA showed highly enhanced redox peaks (oxidation peak current: 32.3 $\mu$A) compared with the other chess-table-like nanostructures, including the flat Au/Ag NEA (22.6 $\mu$A) and Au NEA prepared with only Au deposition (25.4 $\mu$A) (Figure 2d). From the results, we successfully developed the Au NPEA and confirmed its characteristics suitable for electrochemical biosensing and its broad applicability in electrochemistry.

**Detection of SARS-CoV-2 RNA Using an MNM Nanocomplex on the NPEA.** Prior to conducting the electrochemical detection of target SARS-CoV-2 RNA using the MNM nanocomplex on the Au NPEA (Figure 3a), molecular modeling was simulated to verify the formation of the MNM nanocomplex. From the simulated modeling analysis, the formation of an MNM nanocomplex composed of SARS-CoV-2 RNA, sensing probe-1, and Ag ions was verified (Figure 3b). We first verified the formation of the nanobiosensor through the hybridization of components on the Au NPEA using electrochemical impedance spectroscopy (EIS) (Figure S10). Next, electrochemical detection of target single SARS-CoV-2 RNA was conducted by CV by adding 10 pM target single SARS-CoV-2 RNA to sensing probe 1-modified substrates. As we expected, the Au NPEA showed the redox signal enhancing effect derived from intercalated Ag ions located inside the double-stranded nucleic acids (oxidation peak current: 60.6 $\mu$A at around 0.11 V) compared with the other control substrates, including only a Au electrodeposited (Au-ED) substrate (10.4 $\mu$A), Au dot pattern (17.0 $\mu$A), and Au-coated silicon substrate (1.38 $\mu$A) (Figure S8). Then, we decreased the added amount of target single SARS-CoV-2 RNA to evaluate the sensitivity of the nanobiosensor through the measurement of redox peak signal intensity (Figure 3c). By decreasing the added amount of target RNA from 1 $\mu$M to 1 fM, the redox intensity of intercalated Ag ions was proportionally decreased (Figure 3d). Reducing the redox signal is proportional to the amount added, which could be more clearly observed by the cyclic voltammograms divided into two ranges (Figure S9). After several repeated measurements, we obtained the linear response graph of the nanobiosensor upon addition of target RNA from 100 pM to 1 fM, which showed femtomolar level detection sensitivity and excellent reliability ($R^2$ = 0.99) (Figure 3e).

In addition, this nanobiosensor could detect only target RNA selectively and reliably. As shown in Figure 3f and g, redox signals from intercalated Ag ions were measured only in the presence of target RNA (1 nM), and no redox signals were measured in the presence of control nucleic acids. We additionally verified the selective detection property of the nanobiosensor by adding different amounts of target and control sequences (10 pM) (Figure S11). Additionally, as a result of the electrochemical investigation of the prepared


https://doi.org/10.1021/acsnano.1c10824
ACS Nano XXXX, XXX, XXX−XXX

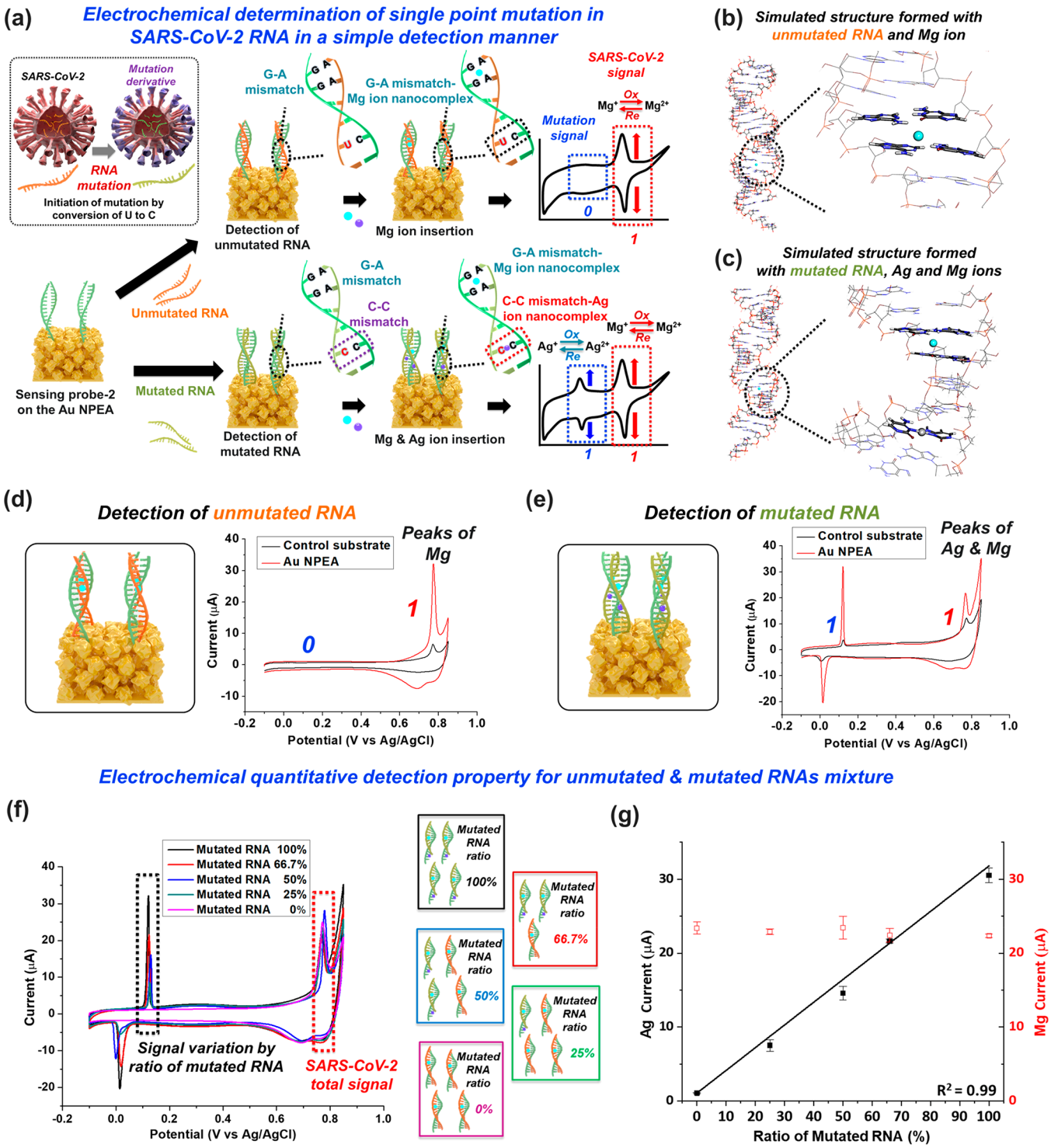


**Figure 4. Electrochemical determination of a single point mutation of SARS-CoV-2 RNA. (a) Schematic diagram of the biosensing mechanism for electrochemical determination of a single point mutation of SARS-CoV-2 RNA. (b, c) Simulated structures and zoomed-in structures of MNM nanocomplexes composed of unmutated RNA, sensing probe-2, and Mg ions (b) and composed of mutated RNA, sensing probe-2, and Ag and Mg ions (c). (d) Cyclic voltammograms of sensing probe-2-modified Au NPEA and the control substrate (flat Au/Ag NEA) in the presence of unmutated RNA. (e) Cyclic voltammograms of sensing probe-2-modified Au NPEA and control substrate (flat Au/Ag NEA) in the presence of mutated RNA. (f) Cyclic voltammograms and (g) linear response plots of the nanobiosensor upon addition of mixtures composed of mutated RNA and unmutated RNA prepared with different ratios (the ratio of mutated RNA: 100%, 66.7%, 50%, 25%, 0%). Error bars show the standard error of the mean of three measurements.**

nanobiosensor by storing at 4 °C every week, our nanobiosensor sufficiently retained its sensing ability (retention of activity: over 95%) for 2 weeks (Figure S12). The stability of our nanobiosensor verified that problems, such as contamination issues, could be avoided during sample preparation and detection processes. With a portable or miniaturized electrochemical instrument, our nanobiosensor could address several critical issues in conventionally used viral detection techniques


https://doi.org/10.1021/acsnano.1c10824
ACS Nano XXXX, XXX, XXX−XXX

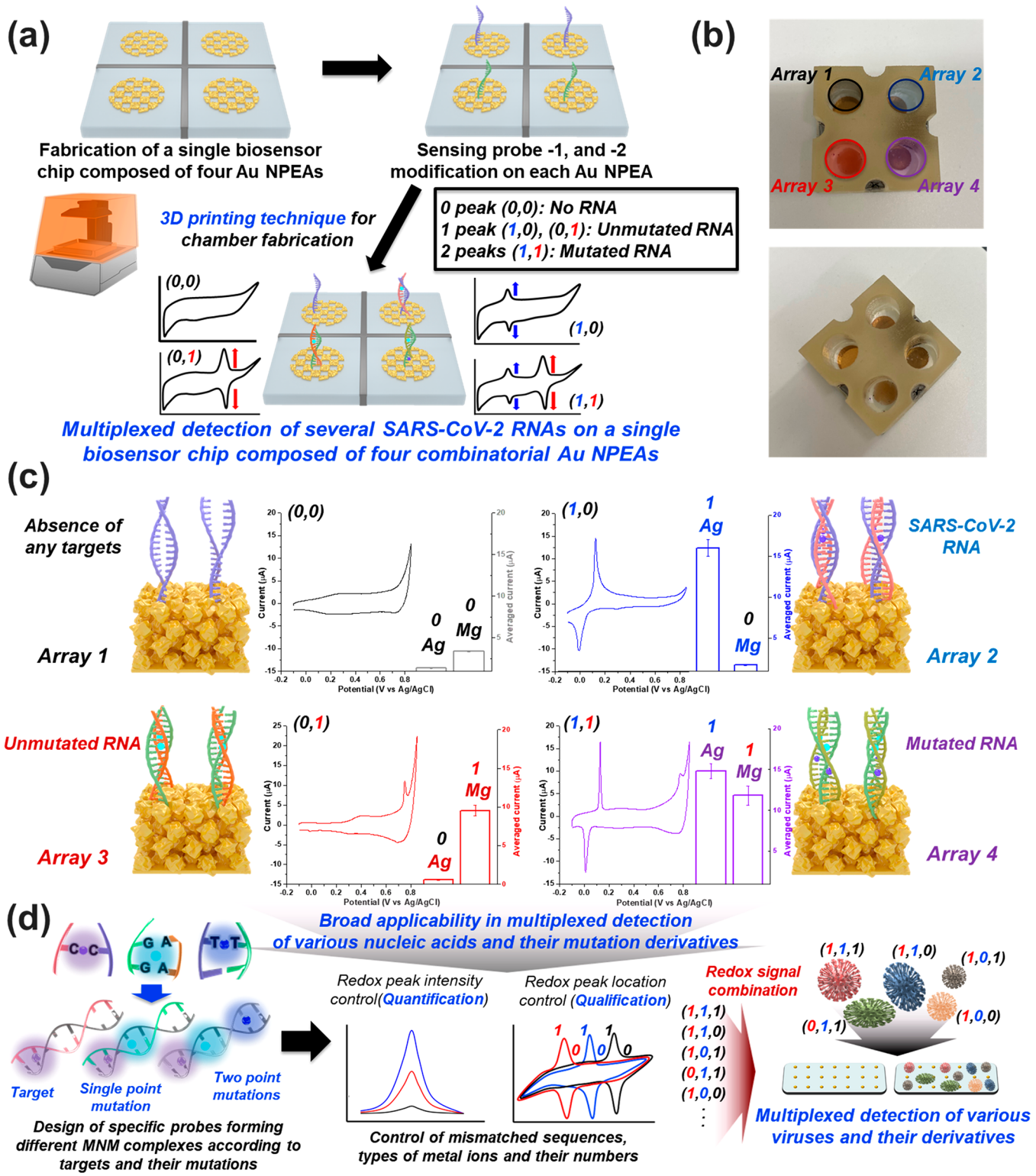


**Figure 5. Multiplexed detection of several SARS-CoV-2 RNAs on the single biosensor chip composed of four combinatorial Au NPEAs. (a) Schematic image of multiplexed detection of several SARS-CoV-2 RNAs on a single biosensor chip composed of four combinatorial Au NPEAs fabricated using a 3D printing technique. (b) Optical images of a 3D-printed chamber-attached single biosensor chip. (c) Cyclic voltammograms and oxidation current peak intensities of each Au NPEA on the single biosensor chip under four different conditions. Error bars show the standard error of the mean of three measurements. (d) Scheme for broad applicability of this nanobiosensor in multiplexed detection of various nucleic acids, viral RNAs, and their mutation derivatives through control of mismatched sequences, metal ions, and numbers by designing sensing probe sequences.**

in cost- and time-effective manners for POC biosensing applications.

**Electrochemical Determination of a Single Point Mutation in SARS-CoV-2 RNA.** On the basis of the MNM



https://doi.org/10.1021/acsnano.1c10824
ACS Nano XXXX, XXX, XXX−XXX

nanocomplex-assisted biosensing mechanism with two different mismatched sequences and metal ions, we next aimed to determine the single point mutation of SARS-CoV-2 RNA using two different sequences of the region causing the D614G mutation in the entire viral SARS-CoV-2 RNA (Figure 4a). First, molecular modeling simulation of two MNM nanocomplexes composed of unmutated RNA or mutated RNA was conducted. Based on simulated structures, MNM nanocomplexes composed of unmutated RNA, sensing probe-2, and Mg ions (Figure 4b) and composed of mutated RNA, sensing probe-2, and Ag and Mg ions (Figure 4c) were verified. After preparing the sensing probe-2-modified Au NPEA, each unmutated RNA and mutated RNA were detected electrochemically by the sensing probe-2. In the presence of unmutated RNA (100 fM), only redox signal from the Mg ion was measured on the sensing probe-2-modified Au NPEA at around 0.77 V as the "1" state with enhanced intensity (oxidation peak current: 32.2 $\mu$A) compared with the signal (oxidation peak current: 6.55 $\mu$A) obtained on the sensing probe-2-modified flat Au/Ag NEA, and redox signal from Ag ions was not measured because of the nonexistence of a C−C mismatched sequence (Figure 4d).

On the other hand, in the presence of mutated RNA (100 fM), two different redox signal pairs from Ag and Mg ions were measured on the sensing probe-2-modified Au NPEA with enhanced intensity (32.1 $\mu$A for Ag ions and 21.9 $\mu$A for Mg ions) compared with those (3.82 $\mu$A for Ag ions and 12.2 $\mu$A for Mg ions) obtained on the flat Au/Ag NEA as both "1" states (Figure 4e). In addition, this biosensor exhibited reproducible detection properties for both unmutated and mutated RNAs. For unmutated RNA detection, this biosensor showed 30.4 and 6.10 $\mu$A of oxidation peak currents of Mg ions on the Au NPEA and on the flat Au/Ag NEA, respectively. For mutated RNA detection, it showed 25.3 and 8.79 $\mu$A of oxidation peak currents of Mg ions on the Au NPEA and on the flat Au/Ag NEA, respectively, and 36.7 and 4.78 $\mu$A of oxidation peak currents of Ag ions on the Au NPEA and on the flat Au/Ag NEA, respectively (Figure S13). Although there was a slight difference in the degree of signal enhancement depending on the types of metal ions, the sensing probe-2-modified Au NPEA distinguished mutated RNA and unmutated RNA with an enhanced redox signal similar to the result for single SARS-CoV-2 RNA detection. The influence of the redox reaction of Ag ions in the altered RNA occurring between the Au NPEA and Mg ions is assumed to be the cause of the difference between the enhanced Mg peak intensities obtained from unmutated RNA and mutated RNA. So, in the case of unmutated RNA detection, the redox reaction of Mg ions was measured by the Au NPEA without any interference from other electrochemical reactions. On the other hand, in the case of mutated RNA, the redox reaction of the Ag ion occurred between the Au NPEA and the Mg ion, which may affect measured redox signals of the Mg ion. As reported in studies in which the redox signal can be affected by other redox reactions existing around the redox source or factors that can affect them,[42,43] the redox reaction of Ag ions may affect the slight decrease of Mg ion peak intensities of mutated RNA. Moreover, we further verified the electrochemical distinction of mutated RNA and unmutated RNA using differential pulse voltammetry (Figure S14). To prove the rapid and simple determination of single point mutation occurrence by the MNM nanocomplex, nanobiosensors prepared without metal ion intercalation were investigated electrochemically (Figure S15). Due to the absence of any reporter molecules in the form of double-stranded nucleic acids, we could not distinguish mutated RNA and unmutated RNA without metal ion intercalation. In contrast, mutated RNA and unmutated RNA were successfully distinguished through redox peak comparison after intercalation of metal ions.

In addition to the qualitative detection property of this nanobiosensor, to investigate the quantitative detection property, the 100 fM mixtures composed of mutated RNA and unmutated RNA prepared with different ratios (the ratio of mutated RNA: 100%, 66.7%, 50%, 25%, 0%) were detected by the sensing probe-2-modified Au NPEA. Since both mutated RNA and unmutated RNA formed the G−A mismatched sequence by hybridization with sensing probe-2, the redox signal intensities of Mg ions were similar in the five conditions (22.3, 22.4, 23.5, 22.9, and 23.4 $\mu$A for 100%, 66.7%, 50%, 25%, and 0%, respectively). However, the redox signal intensity of Ag ions was changed depending on the ratio of mutated RNA, which could only form the C−C mismatched sequence (30.5, 21.6, 14.6, 7.53, and 1.08 $\mu$A for 100%, 66.7%, 50%, 25%, and 0%, respectively) (Figures 4f and S16). As shown in Figure 4g, it showed the reliable linear response of Ag peak signal intensities upon addition of a mixture prepared with different mutated RNA ratios, while maintaining the similar Mg peak signal intensities. From the results, our nanobiosensor could determine the one single point mutation occurrence in a high qualitative and quantitative detection manner, which is desired to determine various viral mutations in clinical applications.

**Multiplexed Detection of Several SARS-CoV-2 RNAs Using a 3D Printing-Assisted Single Biosensor Chip Composed of Four Combinatorial Au NPEAs.** To conduct the multiplexed detection of several SARS-CoV-2 RNAs simultaneously, a single biosensor chip composed of four combinatorial Au NPEAs, to which sensing probes-1 and -2 were immobilized, was fabricated (Figure 5a). First, four Au NPEAs were tightly connected using a colloidal silver paste, and their conductive connection was examined. During the electrochemical investigation, the position of the working electrode was fixed on a prepared single biosensor chip, and electrochemical signals at each Au NPEA containing the redox molecule dissolved electrolyte were measured and exhibited similar cyclic voltammograms in four Au NPEAs, which proved the conductive connection of each Au NPEA (Figure S17). Next, to make a durable single biosensor chip that can be used more broadly, a 3D-printed chamber composed of four holes and a storage region for silver paste on each side was designed and employed on the four Au NPEAs attached to each other (Figure S18). By hardening with silver paste in each storage region, a 3D-printed chamber-attached single biosensor chip composed of four conductively connected Au NPEAs was completed (Figure 5b). After immobilization of sensing probes-1 and -2 on each Au NPEA separately and the addition of three different 10 fM target RNAs (SARS-CoV-2 RNA, unmutated RNA, and mutated RNA), electrochemical multiplexed detection was conducted in real time by fixing the working electrode in one storage region containing the hardened silver paste and moving only the counter and reference electrodes (Figure S18). In terms of the number of redox peaks (Mg ion peak and Ag ion peak) in the current system, no peaks meant the absence of any RNAs (both peaks were Off states as "(0,0)"), one peak (only the Mg peak was


https://doi.org/10.1021/acsnano.1c10824
ACS Nano XXXX, XXX, XXX−XXX

the On state as "(1,0)", or only the Ag peak was the On state as "(0,1)") meant the existence of SARS-CoV-2 RNA without mutation, and two peaks (both Mg and Ag peaks were On states as "(1,1)") meant the mutation occurrence in SARS-CoV-2 RNA.

Figure 5c shows the results obtained from each Au NPEA in four different conditions. The cyclic voltammogram did not show any apparent redox peaks in the first Au NPEA modified with sensing probe-1 (array 1) without any target RNAs. It only showed the threshold oxidation current signals as 1.36 $\mu$A for Ag ions and 3.39 $\mu$A for Mg ions as "(0,0)". In the case of the second Au NPEA modified with sensing probe-1 (array 2), it showed the apparent redox peaks derived from Ag ions (14.5 $\mu$A) in the cyclic voltammogram and showed reliable oxidation current signals as 16.0 $\mu$A for Ag ions in the presence of SARS-CoV-2 RNA as "(1,0)". On the contrary, in the third and fourth Au NPEAs modified with sensing probe-2 (arrays 3 and 4), different graphs were obtained under the influence of intercalated Mg ions due to the input target RNAs (unmutated RNA and mutated RNA). Array 3 showed the cyclic voltammogram possessing only Mg peaks (11.0 $\mu$A) and exhibited reliable oxidation current signals as 9.54 $\mu$A from Mg ions in the presence of unmutated RNA as "(0,1)". In the case of array 4 in which mutated RNA was added, the cyclic voltammogram showed both Ag and Mg peaks (16.4 and 9.45 $\mu$A, respectively) and displayed reliable signals as 14.8 $\mu$A for Ag ions and 11.8 $\mu$A for Mg ions as "(1,1)". In this current multiplexed biosensing system, three different SARS-CoV-2 RNAs were measured in a highly sensitive and selective manner, which provides a promising platform technology that can be applied for simultaneous detection of various nucleic acids, especially viral RNAs and their single point mutations. Moreover, by combining previously reported types of MNM nanocomplexes (C−C for Ag ion, G−A for Mg ion, or T−T for Hg ion),[31,32,34,36] we expect to be able to distinguish up to two point mutations, if we know the detailed sequence information for the specific mutation site of the target viral nucleic acid in which the multiple point mutations have occurred, through the control of several different MNM nanocomplexes by the design of sensing probe sequences and exhibition with at least combined three-digit numbers (*e.g.*, "(1,1,1)", "(0,1,1)", and so on) that are easily distinguished and specified as shown in Figure 5d.

## CONCLUSIONS

The effective detection method of targeted nucleic acids and their mutation derivatives is essential in biological and biomedical science. Moreover, accurate detection of viral nucleic acids and their mutation derivatives in recent infectious viral diseases is much more critical. However, conventional biosensors developed so far typically require several preprocessing steps through complex modifications with a high cost for nucleic acid biosensing. It is challenging to diagnose mutations at the single-nucleotide level, hindering their broad applications for effective viral nucleic acid detection. Therefore, there is a need to develop a reliable and accurate nanobiosensor to detect nucleic acids without target amplifying and tagging processes and to determine the mutation occurrence in a simple detection manner.

Our developed nanobiosensor demonstrated an electrochemical detection of SARS-CoV-2 RNA in highly sensitive, simple, and time-effective manners. In addition, using a simple electrochemical analyzing method, the determination of a single-sequence RNA mutation was validated. Furthermore, multiplexed detection of several SARS-CoV-2 RNAs was successfully conducted simultaneously using a 3D printing technique-mediated single biosensor chip composed of four combinatorial Au NPEAs. This nanobiosensor has potential for POC applications compared with recently reported biosensors because of the absence of target amplification and probe-tagging processes, which reduce time consumption, ease of operation, including the simple dropping of a metal ion solution, and capability of mutation detection, which is of utmost importance worldwide (Table S2). We will further investigate the spacing effect of the Au NPEA and the effect according to the location and numbers of metal ions in the MNM nanocomplex, which can improve its overall sensing efficacy and provide an effective POC biosensing platform by combining with a portable electrochemical device. In conclusion, our electrochemical nucleic acids nanobiosensor can provide a promising platform technology broadly applicable to monitor various nucleic acids, including SARS-CoV-2 RNA, and their mutation derivatives in a simple and the time-effective manner in POC biosensing.

## MATERIALS AND METHODS

**Materials and Reagents.** Thiolated sensing probe-1 (CATTTCGCTGATTTTGCGGTCCCC-thiol), thiolated sensing probe-2 (CCAAGACACGTCAAGGGTCGGCCC-thiol), target single partial SARS-CoV-2 RNA (GACCCCAAAAUCAGCGAAAU), the D614G mutation inducible single point mutated SARS-CoV-2 RNA (mutated RNA) (CCCACAAUUGACGUGUCUUG), unmutation sequence of SARS-CoV-2 RNA (unmutated RNA) (CCUACAAUUGACGUGUCUUG), and the control sequences (AAATAAAAAGGGGGGGGGCGGGGGTT and AAAAATCAAAAAACCCCCG) were ordered from Bioneer (Korea). The ITO-coated glass substrate (15 $\Omega$/cm$^2$, 0.5 mm thickness, active patterning area 1.5 × 1.5 cm$^2$) and the Au substrate composed of Au (50 nm) and Cr (2 nm) on silicon dioxide (5 mm) were purchased from the National Nanofab Center (South Korea). The hexamethyldisilazane (HMDS), tris(2-carboxyethyl)phosphine hydrochloride (TCEP), potassium ferricyanide(III), Triton X-100, and silver nitrate ($AgNO_3$) were purchased from Sigma-Aldrich (USA). The Au and Ag plating solutions and magnesium sulfate ($MgSO_4$) were purchased from Alfa Aesar (USA). The UV-cross-linkable photoresist (AZ2020), PR solvent (AZ EBR solvent), and developer solution (AZ 300 MIF developer) were obtained from Merck KgaA (Germany). The DMSO and nitric acid were purchased from Corning (USA) and Thermo Fisher Scientific (USA), respectively. The Sylgard 184 silicone elastomer base and curing agent for PDMS were purchased from Dow Corning (USA). As the electrolyte, the Dulbecco's phosphate-buffered saline (DPBS, 1×), ethanol, and colloidal silver paste were obtained from Gibco (USA), Decon Laboratories (USA), and Ted Pella Inc. (USA), respectively. Distilled water (DIW) was purified using a Milli-Q machine (Millipore, USA).

**Fabrication of the PR Pattern.** First, the ITO substrate was cleansed by 1% Triton X-100 for 20 min under sonication and washed by ethanol and DIW sequentially for 20 min under sonication. Next, after $O_2$ plasma treatment, HMDS was functionalized on the ITO through vapor phase deposition, and then the PR solution diluted in the PR solvent with the ratio of 1:0.8 was spin-coated on the ITO substrate using a spin-coater (Laurell Technologies, USA). The PR spin-coated substrate was prebaked for 60 s at 100 °C using a hot plate and exposed to UV light ($\lambda$ = 325 nm, 0.81 mW) by the light source (He−Cd laser, Kimmon Koha Laser Systems, Japan). At the same time, the Lloyd's mirror interferometer induced the periodic intensity profiles of the light coming from the source to produce a regular PR pattern on the substrate through a combination of direct incoming light and reflected light from Lloyd's mirror. Based on our previous results, 5.8° was used as the incident angle for forming a


https://doi.org/10.1021/acsnano.1c10824
ACS Nano XXXX, XXX, XXX−XXX

1600 nm pitch sized PR pattern. To make the dot-shaped PR pattern, the PR spin-coated substrate was exposed to UV light once and then exposed again after being rotated 90° for 10 s each exposure. The UV-exposed PR spin-coated substrate was postbaked at 120 °C for 1 min to harden the UV-exposed PR region, and then the PR region not exposed to UV was removed by developer solution for 23 s. Finally, the PR pattern composed of 800 nm sized dots was fabricated on the ITO substrate.

**Fabrication of the Au NPEA and a Single Biosensor Chip Composed of Four Combinatorial Au NPEAs.** To fabricate the Au NPEA, the 3D-printed hole chamber was attached on the dot-shaped PR pattern substrate using PDMS. Next, by using the conventional three-electrodes system composed of a platinum wire electrode as the counter electrode, a silver/silver chloride (Ag/AgCl) double-junction electrode as the reference electrode, and a dot-shaped PR pattern substrate as the working electrode, and the electrochemical deposition was conducted on the dot-shaped PR pattern substrate. First, the electrochemical deposition of Au was conducted by multipotential steps (CHI 600E potentiostat workstation, CH Instruments, Inc., TX, USA) for 45 s under an applied potential of −0.95 V, sample interval of 0.032 s, quiet time of 2 s, and sensitivity of $1.0 \times 10^{-3}$ (A/V) to form the metallic bottom region composed of Au, and then the mixture composed of Au and Ag with the ratio of 6:1 was electrochemically deposited for 20 s under the same conditions to form the chess-table-like flat Au/Ag NEA. Next, the substrate was treated with DMSO to remove the PR pattern, and then the substrate was treated with nitric acids to etch the Ag nanolayer. Finally, the Au NPEA was fabricated on the ITO substrate. The prepared Au NPEA was stored in ethanol until further experimentation. To make a single biosensor chip composed of four combinatorial Au NPEAs, four Au NPEAs were connected to each other (2 × 2 size), and a 3D-printed chamber made with four holes was attached thereon by PDMS. Next, the colloidal silver paste was poured into the reservoir section located on each of the four sides of the chamber to connect the four Au NPEAs conductively. In the final, a single biosensor chip composed of four combinatorial Au NPEAs was developed, and the ethanol was stored in each Au NPEA until further study.

**Characterization of the Au NPEA.** The surface of the prepared Au NPEA, flat Au/Ag NEA, and PR pattern were characterized by field-emission scanning electron microscopy (FE-SEM, Carl Zeiss, Germany) and atomic force microscopy (AFM, NX-10, Park Systems, South Korea). For the PR pattern, the Au was sputtered with 20 nm thickness using a metal ion sputter (KIC-1A, COXEM, South Korea) to form the conductive layer for SEM investigation. During the SEM analysis, EDS analysis was conducted to verify the removal of the Ag nanolayer after the Ag etching process. For AFM analysis, noncontact mode AFM was performed to image the surface of each substrate at a nanometer scale, and by the XEI program, the height profile analysis and 3D images were collected. To confirm the redox signal enhancing property of the Au NPEA, the electrolyte prepared with potassium ferricyanide(III) was used. The redox signals from potassium ferricyanide(III) on the Au NPEA, flat Au/Ag NEA, Au NEA prepared only with Au deposition, Au dot pattern, Au grid pattern, and bare ITO substrate were collected by cyclic voltammetry (CHI 600E potentiostat workstation, CH Instruments, Inc., TX, USA) under a potential range from 0.6 to −0.1 V, a scan rate of 0.05 V/s, a sample interval of 0.001 V, a quiet time of 2 s, and a sensitivity of $1.0 \times 10^{-5}$ (A/V).

**Fabrication of the Nanobiosensor on the Au NPEA.** In order to fabricate the nanobiosensor on the Au NPEA, the prepared Au NPEA was washed with DIW, and the 1 μM of thiolated sensing probe-1 treated with TCEP for cutting of the disulfide bond was immobilized on the Au NPEA for 3 h at 4 °C through the Au−thiol bond. Then, the 1 μM of target single SARS-CoV-2 RNA dissolved in RNase-free water was immobilized on the sensing probe-1-modified Au NPEA for 1 h at 4 °C to form the double-stranded structure with one C−C mismatched sequence. Next, 1 mM $AgNO_3$ was added to the Au NPEA to insert the Ag ions inside the C−C mismatched sequence to form the MNM nanocomplex on the Au NPEA for 30 min at 4 °C. Each immobilization step was conducted after washing with DIW and thoroughly drying by $N_2$ gas. The Au NPEA, sensing probe-1-modified Au NPEA, mismatched dsDNA-modified Au NPEA, and MNM nanocomplex-modified Au NPEA were investigated by EIS investigation using an AC impedance technique (CHI 600E potentiostat workstation) under the initial potential of 0.2 V, high frequency of 1 000 000 Hz, low frequency of 0.01 Hz, amplitude of 0.005 V, and 2 s quiet time to verify the formation of the nanobiosensor on the Au NPEA.

**Electrochemical Detection of Single SARS-CoV-2 RNA.** To conduct the electrochemical detection of target single SARS-CoV-2 RNA, the 1 μM of sensing probe-1-modified Au NPEA was prepared following the above-mentioned protocol. Next, different amounts of target single SARS-CoV-2 RNA (from 1 μM to 1 fM amounts) were immobilized on each sensing probe-1-modified Au NPEA, and then 1 mM $AgNO_3$ was added on the Au NPEA. Each immobilization step was conducted after washing with DIW and thoroughly drying by $N_2$ gas. Prepared nanobiosensors were investigated by CV to estimate the biosensing property for target single SARS-CoV-2 RNA detection. To achieve this, DPBS was used as the electrolyte, and a three-electrode system was utilized for CV investigation. Under a potential range from 0.6 to −0.1 V, the scan rate of 0.05 V/s, sample interval of 0.001 V, quiet time of 2 s, and sensitivity of $1.0 \times 10^{-5}$ (A/V), redox signals from Ag ions intercalated inside the C−C mismatched sequence were collected. For comparison, nanobiosensors were prepared on the Au dot pattern, Au electrochemical deposited (ED) ITO substrate, and Au-coated silicon substrate and investigated by CV under the same conditions. For investigation of the sensitive detection property of the nanobiosensor, the control sequences (AAATAAAAA-GGGGGGGGGCGGGGGTT and AAAAATCAAAAAACCCCCG), instead of target single SARS-CoV-2 RNA, were immobilized on the 1 μM of sensing probe-1-modified Au NPEA and investigated by CV after $AgNO_3$ addition. Lastly, to investigate the stability of the nanobiosensor, the prepared nanobiosensor was stored at 4 °C and investigated by CV every week.

**Electrochemical Determination of a Single Point Mutation of SARS-CoV-2 RNA.** To conduct the electrochemical determination of single point mutation of SARS-CoV-2 RNA, we selected the D614G mutation inducible single point mutated SARS-CoV-2 RNA (mutated RNA) as the target mutation. First, the 1 μM of sensing probe-2-modified Au NPEA was prepared in the same way as the previous experiments, and then, the 100 fM of mutated RNA and unmutation sequence of SARS-CoV-2 RNA (unmutated RNA) were immobilized on the sensing probe-2-modified Au NPEA, respectively. After forming each nucleic acid on the Au NPEA, 1 mM $AgNO_3$ and 1 mM $MgSO_4$ were added in order. Each immobilization step was conducted after washing with DIW and thoroughly drying by $N_2$ gas. To detect and distinguish the mutated RNA and unmutated RNA for mutation occurrence determination, each prepared nanobiosensor was investigated by CV under a potential range from 0.85 to −0.1 V, a scan rate of 0.05 V/s, a sample interval of 0.001 V, a quiet time of 2 s, and a sensitivity of $1.0 \times 10^{-5}$ (A/V) to obtain the Ag and Mg redox signals from a mutated RNA immobilized nanobiosensor, and the Ag redox signals from an unmutated RNA immobilized nanobiosensor. For verifying the redox signal enhancing effect of Au NPEA, samples prepared in the same manner on the flat Au/Ag NEA substrate were also investigated by CV. Using the same nanobiosensors, differential purse voltammetry (DPV) was performed for additional confirmation of mutation occurrence determination electrochemically. To operate the DPV, a potential range from −0.1 to 0.9 V, a potential increase of 0.004 V, an amplitude of 0.05 V, a pulse width of 0.05 s, a sampling width of 0.0167 s, a pulse period of 0.5 s, a quiet time of 2 s, and a sensitivity of $1.0 \times 10^{-5}$ (A/V) were applied. Next, to evaluate the quantification property of the nanobiosensor, the 100 fM mixtures composed of mutated RNA and unmutated RNA prepared with different ratios (100%, 66.7%, 50%, 25%, and 0% ratio of mutated RNA) were immobilized on the sensing probe-2-modified Au NPEA, and then, 1 mM $AgNO_3$ and 1 mM $MgSO_4$ were added sequentially. The redox signal intensities from Ag and Mg ions were collected and analyzed by CV under the same conditions.


https://doi.org/10.1021/acsnano.1c10824
ACS Nano XXXX, XXX, XXX−XXX

**Multiplexed Detection of Several SARS-CoV-2 RNAs a Single Biosensor Chip Composed of Four Combinatorial Au NPEAs.** To conduct the multiplexed detection of several SARS-CoV-2 RNAs on a single biosensor chip composed of four combinatorial Au NPEAs, we verified the conductive connection of four Au NPEAs using colloidal silver paste. To achieve this, by using potassium ferricyanide(III) in each connected Au NPEA, redox signals from each Au NPEA were measured. During the measurement, a single biosensor chip was used as one working electrode, and only reference and counter electrodes were moved in each Au NPEA for collecting the redox signals from each Au NPEA. After verification of the conductive connection of the four Au NPEAs, the 1 $\mu$M of sensing probe-1 and sensing probe-2 were modified on two Au NPEAs, each on the single biosensor chip (sensing probe-1 on array 1 and 2 and sensing probe-2 on arrays 3 and 4). Next, several SARS-CoV-2 RNAs, including the single SARS-CoV-2 RNA, mutated RNA, and unmutated RNA, were added on each Au NPEA, respectively. For multiplexed electrochemical detection, CV was conducted under a potential range from 0.85 to −0.1 V, a scan rate of 0.05 V/s, a sample interval of 0.001 V, a quiet time of 2 s, and a sensitivity of $1.0 \times 10^{-5}$ (A/V) by only moving the reference and counter electrodes in each Au NPEA.

## ASSOCIATED CONTENT

### Supporting Information

The Supporting Information is available free of charge at https://pubs.acs.org/doi/10.1021/acsnano.1c10824.

Additional results and discussion, surface morphologies of PR patterns, 3D images and height profiles of PR patterns, (a) Scheme and optical image of a 3D printed hole chamber. (b) Optical images for the operation of electrochemical deposition. (c) Cyclic voltammograms of potassium ferricyanide (III). (d) Electrochemical deposition graphs of Au and Au/Ag mixture, (a,b) SEM images of Au NPEAs prepared with different ratios, (a−c) SEM images of PR pattern, flat Au/Ag NEA, and Au NPEA, (a−c) AFM images and surface profiles, (a,b) EDS analysis results, (a) cyclic voltammograms from intercalated Ag ions. (b) Averaged oxidation peak current intensities of intercalated Ag ions, (a,b) Cyclic voltammograms upon addition of target single SARS-CoV-2 RNA, schematic diagram of nanobiosensor fabrication, and Nyquist plots, (a) Cyclic voltammograms in the presence of target single SARS-CoV-2 RNA and control sequence. (b) Averaged oxidation current peak intensities in the presence of target single SARS-CoV-2 RNA and control sequences, (a,b) Averaged oxidation current peak intensities for 2 weeks, (a,b) Oxidation current peak intensities in the presence of unmutated RNA or mutated RNA (b), (a,b) Differential pulse voltammograms in the presence of unmutated RNA or mutated RNA, (a,b) Cyclic voltammograms without metal ions intercalation or with metal ions intercalation, Oxidation current peak intensities upon adding mixtures composed of mutated RNA and unmutated RNA, (a) Optical image of four Au NPEAs connected by using colloidal silver paster. (b−e) Cyclic voltammograms obtained from Array 1, Array 2, Array 3, and Array 4, scheme and optical images of a 3D printed chamber, and optical images for operation of electrochemical multiplexed detection, sequence information, comparison table. Supplementary Figures 1−18, Supplementary Tables 1 and 2 (PDF)

## AUTHOR INFORMATION


### Corresponding Authors

**Jeong-Woo Choi** − *Department of Chemical & Biomolecular Engineering, Sogang University, Mapo-gu, Seoul 04107, Republic of Korea;* orcid.org/0000-0003-0100-0582; Email: jwchoi@sogang.ac.kr; http://home.sogang.ac.kr/sites/nbel/

**Ki-Bum Lee** − *Department of Chemistry and Chemical Biology, Rutgers, The State University of New Jersey, Piscataway, New Jersey 08854, United States;* orcid.org/0000-0002-8164-0047; Email: kblee@rutgers.edu; https://kblee.rutgers.edu/

### Authors

**Jinho Yoon** − *Department of Chemistry and Chemical Biology, Rutgers, The State University of New Jersey, Piscataway, New Jersey 08854, United States; Department of Chemical & Biomolecular Engineering, Sogang University, Mapo-gu, Seoul 04107, Republic of Korea;* orcid.org/0000-0003-4614-9217

**Brian M. Conley** − *Department of Chemistry and Chemical Biology, Rutgers, The State University of New Jersey, Piscataway, New Jersey 08854, United States*

**Minkyu Shin** − *Department of Chemical & Biomolecular Engineering, Sogang University, Mapo-gu, Seoul 04107, Republic of Korea*

**Jin-Ha Choi** − *School of Chemical Engineering, Jeonbuk National University, Jeollabuk-do 54896, Republic of Korea;* orcid.org/0000-0002-1632-9586

**Cemile Kilic Bektas** − *Department of Chemistry and Chemical Biology, Rutgers, The State University of New Jersey, Piscataway, New Jersey 08854, United States*

Complete contact information is available at: https://pubs.acs.org/10.1021/acsnano.1c10824


### Author Contributions

J.Y., J.-H.C., and K.-B.L. initially designed the concept. J.Y., J.-W.C., and K.-B.L. organized the structure of the experimental design and manuscript. J.Y., B.C., M.S., and C.K.B. conducted all experiments. J.Y., J.-W.C., and K.-B.L. wrote the manuscript. J.-W.C. and K.-B.L. directed the entire research. All authors have read and agreed to the published version of the manuscript.

### Notes

The authors declare no competing financial interest.

## ACKNOWLEDGMENTS

K.-B.L. acknowledges the partial financial support from the NSF (CHE-1429062), the NJHF Grant (#PC16-21CV), and the Rutgers Global Health Grant. J.-W.C. acknowledges the partial financial support from the National Research Foundation of Korea (NRF) grant funded by the Korean government (MSIT) (2019R1A2C3002300) and the National R&D Program through the National Research Foundation of Korea (NRF) funded by the Ministry of Science and ICT (NRF-2022M3H4A1A01005271). J.Y. acknowledges support from New Jersey Commission on Cancer Research (SNJ-CCR-DCHS20PPC043). The authors are also grateful to Jihye Yeom for MNM nanocomplex structure simulation.

## REFERENCES


(1) Greve, T. S.; Judson, R. L.; Blelloch, R. microRNA control of mouse and human pluripotent stem cell behavior. *Annu. Rev. Cell Dev. Biol.* **2013**, *29* (1), 213−239.

(2) Tateishi-Karimata, H.; Sugimoto, N. Roles of non-canonical structures of nucleic acids in cancer and neurodegenerative diseases. *Nucleic Acids Res.* **2011**, *49* (14), 7839−7855.

(3) Samanta, D.; Ebrahimi, S. B.; Mirkin, C. A. Nucleic-Acid Structures as Intracellular Probes for Live Cells. *Adv. Mater.* **2020**, *32* (13), 1901743.

(4) Guo, C.; Ding, P.; Xie, C.; Ye, C.; Ye, M.; Pan, C.; Cao, X.; Zhang, S.; Zheng, S. Potential application of the oxidative nucleic acid damage biomarkers in detection of diseases. *Oncotarget* **2017**, *8* (43), 75767−75777.

(5) Opalinska, J. B.; Gewirtz, A. M. Nucleic-acid therapeutics: basic principles and recent applications. *Nat. Rev. Drug Discovery* **2002**, *1* (7), 503−514.

(6) Shen, M.; Zhou, Y.; Ye, J.; AL-maskri, A. A. A.; Kang, Y.; Zeng, S.; Cai, S. Recent advances and perspectives of nucleic acid detection for coronavirus. *J. Pharm. Anal.* **2020**, *10* (2), 97−101.

(7) Coronaviridae Study Group of the International Committee on Taxonomy of Viruses, The species Severe acute respiratory syndrome-related coronavirus: classifying 2019-nCoV and naming it SARS-CoV-2. *Nat. Microbiol.* **2020**, *5*, 536−544.

(8) Hu, B.; Guo, H.; Zhou, P.; Shi, Z.-L. Characteristics of SARS-CoV-2 and COVID-19. *Nat. Rev. Microbiol.* **2021**, *19* (3), 141−154.

(9) Shaw, W. H.; Lin, Q.; Muhammad, Z. Z. B. R.; Lee, J. J.; Khong, W. X.; Ng, O. T.; Tan, E. L.; Li, P. Identification of HIV Mutation as Diagnostic Biomarker through Next Generation Sequencing. *J. Clin. Diagn. Res.* **2016**, *10* (7), DC04−DC08.

(10) Sanjuán, R.; Domingo-Calap, P. Mechanisms of viral mutation. *Cell. Mol. Life Sci.* **2016**, *73* (23), 4433−4448.

(11) Xie, B.-P.; Qiu, G.-H.; Hu, P.-P.; Liang, Z.; Liang, Y.-M.; Sun, B.; Bai, L.-P.; Jiang, Z.-H.; Chen, J.-X. Simultaneous detection of Dengue and Zika virus RNA sequences with a three-dimensional Cu-based zwitterionic metal−organic framework, comparison of single and synchronous fluorescence analysis. *Sens. Actuators B Chem.* **2018**, *254*, 1133−1140.

(12) Adegoke, O.; Morita, M.; Kato, T.; Ito, M.; Suzuki, T.; Park, E. Y. Localized surface plasmon resonance-mediated fluorescence signals in plasmonic nanoparticle-quantum dot hybrids for ultrasensitive Zika virus RNA detection via hairpin hybridization. *Biosens. Bioelectron.* **2017**, *94*, 513−522.

(13) He, Y.; Yang, X.; Yuan, R.; Chai, Y. A novel ratiometric SERS biosensor with one Raman probe for ultrasensitive microRNA detection based on DNA hydrogel amplification. *J. Mater. Chem. B* **2019**, *7* (16), 2643−2647.

(14) Tavallaie, R.; McCarroll, J.; Le Grand, M.; Ariotti, N.; Schuhmann, W.; Bakker, E.; Tilley, R. D.; Hibbert, D. B.; Kavallaris, M.; Gooding, J. J. Nucleic acid hybridization on an electrically reconfigurable network of gold-coated magnetic nanoparticles enables microRNA detection in blood. *Nat. Nanotechnol.* **2018**, *13* (11), 1066−1071.

(15) Ge, Z.; Lin, M.; Wang, P.; Pei, H.; Yan, J.; Shi, J.; Huang, Q.; He, D.; Fan, C.; Zuo, X. Hybridization chain reaction amplification of microRNA detection with a tetrahedral DNA nanostructure-based electrochemical biosensor. *Anal. Chem.* **2014**, *86* (4), 2124−2130.

(16) Qiu, G.; Gai, Z.; Tao, Y.; Schmitt, J.; Kullak-Ublick, G. A.; Wang, J. Dual-Functional Plasmonic Photothermal Biosensors for Highly Accurate Severe Acute Respiratory Syndrome Coronavirus 2 Detection. *ACS Nano* **2020**, *14* (5), 5268−5277.

(17) Xu, W.; Jin, T.; Dai, Y.; Liu, C. C. Surpassing the detection limit and accuracy of the electrochemical DNA sensor through the application of CRISPR Cas systems. *Biosens. Bioelectron.* **2020**, *155*, 112100.

(18) Lee, T.; Mohammadniaei, M.; Zhang, H.; Yoon, J.; Choi, H. K.; Guo, S.; Guo, P.; Choi, J.-W. Single Functionalized pRNA/Gold Nanoparticle for Ultrasensitive MicroRNA Detection Using Electrochemical Surface-Enhanced Raman Spectroscopy. *Adv. Sci.* **2020**, *7* (3), 1902477.

(19) Su, Y.; Hammond, M. C. RNA-Based Fluorescent Biosensors for Live Cell Imaging of Small Molecules and RNAs. *Curr. Opin. Biotechnol.* **2020**, *63*, 157−166.

(20) Zarei, M. Portable biosensing devices for point-of-care diagnostics: Recent developments and applications. *Trends Anal. Chem.* **2017**, *91*, 26−41.

(21) Han, G.-R.; Koo, H. J.; Ki, H.; Kim, M.-G. Paper/Soluble Polymer Hybrid-Based Lateral Flow Biosensing Platform for High-Performance Point-of-Care Testing. *ACS Appl. Mater. Interfaces* **2020**, *12* (31), 34564−34575.

(22) Jungreis, I.; Sealfon, R.; Kellis, M. SARS-CoV-2 gene content and COVID-19 mutation impact by comparing 44 Sarbecovirus genomes. *Nat. Commun.* **2021**, *12* (1), 2642.

(23) Harris, T. D.; Buzby, P. R.; Babcock, H.; Beer, E.; Bowers, J.; Braslavsky, I.; Causey, M.; Colonell, J.; DiMeo, J.; Efcavitch, J. W.; Giladi, E.; Gill, J.; Healy, J.; Jarosz, M.; Lapen, D.; Moulton, K.; Quake, S. R.; Steinmann, K.; Thayer, E.; Tyurina, A.; Ward, R.; Weiss, H.; Xie, Z. Single-Molecule DNA Sequencing of a Viral Genome. *Science* **2008**, *320* (5872), 106−109.

(24) Dai, Y.; Liu, C. C. Recent Advances on Electrochemical Biosensing Strategies toward Universal Point-of-Care Systems. *Angew. Chem., Int. Ed.* **2019**, *58* (36), 12355−12368.

(25) Khan, M. Z. H.; Hasan, M. R.; Hossain, S. I.; Ahommed, M. S.; Daizy, M. Ultrasensitive detection of pathogenic viruses with electrochemical biosensor: State of the art. *Biosens. Bioelectron.* **2020**, *166*, 112431.

(26) Young, S. L.; Kellon, J. E.; Hutchison, J. E. Small Gold Nanoparticles Interfaced to Electrodes through Molecular Linkers: A Platform to Enhance Electron Transfer and Increase Electrochemically Active Surface Area. *J. Am. Chem. Soc.* **2016**, *138* (42), 13975−13984.

(27) Biener, J.; Wittstock, A.; Zepeda-Ruiz, L. A.; Biener, M. M.; Zielasek, V.; Kramer, D.; Viswanath, R. N.; Weissmüller, J.; Bäumer, M.; Hamza, A. V. Surface-chemistry-driven actuation in nanoporous gold. *Nat. Mater.* **2009**, *8* (1), 47−51.

(28) Lee, J.-H.; Choi, H. K.; Yang, L.; Chueng, S. -T. D.; Choi, J.-W.; Lee, K.-B. Nondestructive Real-Time Monitoring of Enhanced Stem Cell Differentiation Using a Graphene-Au Hybrid Nanoelectrode Array. *Adv. Mater.* **2018**, *30* (39), 1802762.

(29) Kim, T.-H.; Yea, C.-H.; Chueng, S. -T. D.; Yin, P. T. -T.; Conley, B.; Dardir, K.; Pak, Y.; Jung, G. Y.; J Choi, J.-W.; Lee, K.-B. Large-Scale Nanoelectrode Arrays to Monitor the Dopaminergic Differentiation of Human Neural Stem Cells. *Adv. Mater.* **2015**, *27* (41), 6356−6362.

(30) Tanaka, K.; Clever, G. H.; Takezawa, Y.; Yamada, Y.; Kaul, C.; Shionoya, M.; Carell, T. Programmable self-assembly of metal ions inside artificial DNA duplexes. *Nat. Nanotechnol.* **2006**, *1* (3), 190−194.

(31) Ono, A.; Torigoe, H.; Tanaka, Y.; Okamoto, I. Binding of metal ions by pyrimidine base pairs in DNA duplexes. *Chem. Soc. Rev.* **2011**, *40* (12), 5855−5866.

(32) Okamoto, I.; Iwamoto, K.; Watanabe, Y.; Miyake, Y.; Ono, A. Metal-Ion Selectivity of Chemically Modified Uracil Pairs in DNA Duplexes. *Angew. Chem., Int. Ed.* **2009**, *48* (9), 1648−1651.

(33) Mohammadniaei, M.; Yoon, J.; Lee, T.; Bharate, B. G.; Jo, J.; Lee, D.; Choi, J.-W. Electrochemical Biosensor Composed of Silver Ion-Mediated dsDNA on Au-Encapsulated $Bi_2Se_3$ Nanoparticles for the Detection of $H_2O_2$ Released from Breast Cancer Cells. *Small* **2018**, *14* (16), 1703970.

(34) Rüdisser, S.; Tinoco, I., Jr Solution structure of Cobalt(III)-hexammine complexed to the GAAA tetraloop, and metal-ion binding to G.A mismatches. *J. Mol. Biol.* **2000**, *295* (5), 1211−1223.

(35) Ono, A.; Cao, S.; Togashi, H.; Tashiro, M.; Fujimoto, T.; Machinami, T.; Oda, S.; Miyake, Y.; Okamoto, I.; Tanaka, Y. Specific interactions between silver(i) ions and cytosine−cytosine pairs in DNA duplexes. *Chem. Commun.* **2008**, 4825−4827.




https://doi.org/10.1021/acsnano.1c10824
*ACS Nano* XXXX, XXX, XXX−XXX

(36) Zhao, Q.; Nagaswamy, U.; Lee, H.; Xia, Y.; Huang, H.-C.; Gao, X.; Fox, G. E. NMR structure and $Mg^{2+}$ binding of an RNA segment that underlies the L7/L12 stalk in the E.coli 50S ribosomal subunit. *Nucleic Acids Res.* **2005**, *33* (10), 3145−3153.
(37) Mohammadniaei, M.; Lee, T.; Yoon, J.; Lee, D.; Choi, J.-W. Electrochemical nucleic acid detection based on parallel structural dsDNA/recombinant azurin hybrid. *Biosens. Bioelectron.* **2017**, *98*, 292−298.
(38) Deng, X.; Xu, Y.; An, Q.; Xiong, F.; Tan, S.; Wu, L.; Mai, L. Manganese ion pre-intercalated hydrated vanadium oxide as a high-performance cathode for magnesium ion batteries. *J. Mater. Chem. A* **2019**, *7* (17), 10644−10650.
(39) Zhu, C.; He, G.; Yin, Q.; Zeng, L.; Ye, X.; Shi, Y.; Xu, W. Molecular biology of the SARs-CoV-2 spike protein: A review of current knowledge. *J. Med. Virol.* **2021**, *93* (10), 5729−5741.
(40) Plante, J. A.; Liu, Y.; Liu, J.; Xia, H.; Johnson, B. A.; Lokugamage, K. G.; Zhang, X.; Muruato, A. E.; Zou, J.; Fontes-Garfias, C. R.; Mirchandani, D.; Scharton, D.; Bilello, J. P.; Ku, Z.; An, Z.; Kalveram, B.; Freiberg, A. N.; Menachery, V. D.; Xie, X.; Plante, K. S.; Weaver, S. C.; Shi, P.-Y. Spike mutation D614G alters SARS-CoV-2 fitness. *Nature* **2021**, *592* (7852), 116−121.
(41) Ozono, S.; Zhang, Y.; Ode, H.; Sano, K.; Tan, T. S.; Imai, K.; Miyoshi, K.; Kishigami, S.; Ueno, T.; Iwatani, Y.; Suzuki, T.; Tokunaga, K. SARS-CoV-2 D614G spike mutation increases entry efficiency with enhanced ACE2-binding affinity. *Nat. Commun.* **2021**, *12* (1), 848.
(42) Lee, T.; Yagati, A. K.; Min, J.; Choi, J.-W. Bioprocessing Device Composed of Protein/DNA/Inorganic Material Hybrid. *Adv. Funct. Mater.* **2014**, *24* (12), 1781−1789.
(43) Lee, T.; Yoo, S.-Y.; Chung, Y.-H.; Min, J.; Choi, J.-W. Signal Enhancement of Electrochemical Biomemory Device Composed of Recombinant Azurin/Gold Nanoparticle. *Electroanalysis* **2011**, *23* (9), 2023−2029.


https://doi.org/10.1021/acsnano.1c10824
*ACS Nano* XXXX, XXX, XXX−XXX